Journal of Hazardous Materials 179 (2010) 642–649

Contents lists available at ScienceDirect

Journal of Hazardous Materials

journal homepage: www.elsevier.com/locate/jhazmat

Adsorption of Cu^{2+} on spherical Fe-MCM-41 and its application for oxidation of adamantane

K.M. Parida [a,*], Suresh K. Dash [b]

[a] Colloids and Material Chemistry Department, Institute of Minerals and Materials, Technology (CSIR), Bhubaneswar 751013, Orissa, India
[b] Department of Chemistry, Institute of Technical Education and Research, SOA University, Bhubaneswar 751030, Orissa, India

ARTICLE INFO

Article history:
Received 3 November 2009
Received in revised form 10 March 2010
Accepted 12 March 2010
Available online 19 March 2010

Keywords:
Fe-MCM-41
Cu^{2+} adsorption
Oxidation
Adamantane

ABSTRACT

Fe-MCM-41 with varying Si/Fe ratios (20, 50, 70 and 90) were prepared by using cetyltrimethylammoniumbromide (CTAB) as the structure-directing agent (SDA), tetraethylorthosilicate (TEOS) as the silica source and ethanol as co-surfactant in alkaline medium. The characterization was done by SEM; UV–vis diffused reflectance and FT-IR. Adsorption of copper solutions with varying parameters such as concentration, temperature and pH were performed over Fe-MCM-41 samples. The experimental data fitted well to the Langmuir and Freundlich adsorption isotherm. Fe-MCM-41 having Si/Fe ratio (90) showed highest copper adsorption capacity at pH 5.5, Cu^{2+} concentration of 59.6 ppm and temperature 323 K. Fe-MCM-41(90)–Cu(59.6) was tested as a catalyst for oxidation of adamantane using hydrogen peroxide as the oxidant. The GC analyses revealed significant conversion of 32.5% and selectivity of 54% towards formation of 1-adamantanol.

1. Introduction

A large number of techniques have been adopted to remove toxic heavy metal ions from wastewater, produced by mining, refining and from industrial effluents like textile, paint and dyes. Though the presence of copper in water and eatables in very low concentrations is favorable for oxygen transport in human physiology, a high concentration leads to fatal consequences. Like other heavy metals, Cu^{2+} has high affinity for ligands containing nitrogen and sulfur donors; hence its toxicity is exerted on enzymes and nucleic acids of human physiology [1]. This leads to haemolysis, damage of liver and kidney and fever with influenza.

The removal of copper from aqueous state by a simple and economically viable method has been a great concern [2]. Reverse osmosis, ion exchange, nano-filtration are some expensive and cumbersome methods for the removal of aqueous toxic ions [3]. Adsorption processes have become more popular for its simplicity and economic viability. However, the structural and chemical heterogeneous nature and multiple adsorption sites of varying accessibility of metal ions are drawbacks with the common sorbents like carbon, clays, biomass, chitosan, etc. Since the discovery of mesoporous molecular sieves MCM-41 by Beck et al. [4] in 1992, many modifications of MCM-41 with metals have been performed for attaining higher activities for adsorption and catalysis [5,6]. But the tunable pore sizes of 2–10 nm and superficial large surface areas extending up to 1000 m^2/g makes MCM-41 an interesting support material for adsorption [7–9].

Incorporation of trivalent atoms into the walls of MCM-41 develops negative centers or Bronsted acid sites that enhance the activities of the material towards adsorption and catalysis [10–12]. In 1997, Unger and co-workers reported the synthesis of submicron spherical MCM-41. Spherical particles are often considered ideal for the adsorption study, but unfortunately the pores vary along with radius of the spherical MCM-41 [13]. These authors further concluded that the addition of alcohol (which works as co-surfactant) to the reacting mixture led to homogeneous crystallization system favoring the formation of spherical MCM-41. MCM-41 silicates proved to be active in oxidation of hydrocarbons [14]. The synthesis and characterization of iron incorporated MCM-41 (Fe-MCM-41) and its catalytic properties have been investigated by Wang et al. [15]. During synthesis, the loading of iron into MCM-41 was up to 1.8% by both direct hydrothermal method and template ion exchange method. Samanta et al. synthesized iron-rich Fe-MCM-41 with a higher loading around 8–10% [16]. The spherical Fe-MCM-41 was synthesized and reviewed by Szegedi et al. [17], where the formation of iron hydroxides and oxides was restricted and the loading of iron into the framework was also highlighted. The higher stability of Fe-MCM-41 was verified under temperature programmed reduction studies that showed the reduction of Fe^{3+} to Fe^0 was only 3%. Though the catalytic study and conversion into beta iron by Fe-MCM-41 has been reported [18], the negative centers were rarely exploited for catalytic activity in chemical reactions after removing heavy metal toxic ions.

* Corresponding author. Tel.: +91 674 2581636x425; fax: +91 674 2581637.
E-mail addresses: paridakulamani@yahoo.com, kmparida@immt.res.in (K.M. Parida).

0304-3894/$ – see front matter © 2010 Elsevier B.V. All rights reserved.
doi:10.1016/j.jhazmat.2010.03.051

The oxidation of cyclohexane at 373 K [19] and sulfur dioxide at 800–1100 K [20] using Fe-MCM-41 as catalyst, has established the thermal stability (1023 K) of the catalyst. Lam's group is among the pioneers to study the removal of Cu^{2+} from aqueous state by mesoporous materials [21,22]. The rate of access to binding sites of Cu^{2+} onto organically modified mesoporous silica and its redox properties were reported earlier [23,24]. The removal of copper from wastewater has been tried by amino-functionalized mesoporous silica [25,26]. These copper loaded materials can be used as an oxidation catalyst; but no such study has been made yet in this aspect. The oxidation of adamantane is of immense importance as its oxidized products (2-adamantanol and 2-adamantanone) have extensive applications in pharmaceutical, agricultural chemicals, semiconductors and optical materials. Both the products are used as raw materials for anticancer drugs and cerebral-function improving agents [27,28].

This reaction is often used as a probe to measure C–H bond activation capacity by various catalysts. Trissa et al. [29] have studied this reaction using urea hydro peroxide (UHP) as the oxidant and vanadium complex anchored functionalized silica as catalyst. The oxidation of adamantane by H_2O_2 using iron polynitroporphyrins as a catalyst was also reported [30]. In the present paper we have used Fe^{3+} incorporated MCM-41 as an adsorbent for removal of toxic Cu^{2+} ions from aqueous solution and also used the copper enriched Fe-MCM-41 as an efficient catalyst for oxidation of adamantane. Here in, we have tried to solve two aspects: (I) removal of toxic copper from aqueous system using Fe-MCM-41 and (II) utilization of Cu^{+2} adsorbed Fe-MCM-41 as an active and selective catalyst for oxidation of adamantane. The effects of different amounts of iron, adsorption temperature, pH influence on the adsorption process, were also examined and the results are discussed in the paper.

2. Experimental

2.1. Preparation of mesoporous Fe-MCM-41

Different amounts of iron incorporated spherical MCM-41 were prepared by slightly modifying the original procedure in order to avoid the formation of iron oxide and iron hydroxide precipitates in alkaline medium at pH 8.0–8.5 [14]. Tetraethylorthosilicate (TEOS, Aldrich, India) was used as the silica source for all syntheses. The cationic surfactant cetyltrimethylammoniumbromide (CTAB, Aldrich, India) was used as the structure-directing group. Nonahydrate ferricnitrate, Fe $(NO_3)_3{\cdot}9H_2O$ (Acros) salt was used for iron modification. CTAB, water, ethanol and TEOS were mixed in the proportion of 1 TEOS:0.3 CTAB:144 H_2O:58 EtOH. To that milky solution, 0.46, 0.18, 0.13 and 0.101 g of $Fe(NO_3)_3{\cdot}9H_2O$ were added (where the Si/Fe ratios were 20, 50, 70 and 90, respectively.) and stirred for 30 min resulting in a light yellow, clear solution. To that ammonia (3.7 ml) was added at one time causing immediate gel precipitation. The color of the precipitate was pale beige. Template removal was performed by calcining at 790 K. Herein after, the samples are named as Fe-MCM-41(xx) (xx = 20, 50, 70 and 90, corresponding to the Si/Fe ratios mentioned above) for as-synthesized materials. The synthesis of MCM-41 was carried out as mentioned elsewhere [2].

2.2. Preparation of adsorbate and batch mode studies

A stock solution of copper nitrate, $Cu(NO_3)_2{\cdot}3H_2O$ (Merck) was prepared with 0.01 M conc. (approx. 534 ppm) by taking 0.2416 g in 100 ml deionized water. Different concentrations of Cu-solutions were prepared (0.001, 0.0025 and 0.005 M) by diluting the stock solution with deionized water. The copper solutions were stamped as Cu(yy) (where yy = 59.6, 153, 272 and 534 ppm). The copper adsorption process in aqueous solution was studied with varying temperatures 303, 313 and 323 K in a shaker bath. The influence of pH on adsorption of copper by Fe-MCM-41(xx) was determined by ELICO pH meter. The pH ranges of 2.5, 3.5, 4.5 and 5.5 were obtained by drop wise addition of dilute HCl. The alkaline pH was obtained by the addition of diluted ammonia solution as addition of NaOH destroys the orderness of Fe-MCM-41 [17].

2.3. Adsorption experiments

A fixed amount of Fe-MCM-41 (0.02 g) was placed in stopper conical flasks, to which 20 ml of Cu-solutions of different concentrations were added. The mixture was stirred for 4 h with a magnetic stirrer and centrifuged [7]. The copper adsorbed materials were collected and dried at 383 K for catalytic activity measurement, whereas Cu concentration in the filtrate was analyzed by AAS (Perkin-Elmer Analyser AA300). The difference with original concentration determined the amount of Cu adsorbed. The AAS was calibrated against standards before each analysis. The equilibrium adsorption capacity was calculated [8] from the following Eq. (1):

$$q_e = \frac{(C_0 - C_e)V}{m} \quad (1)$$

where q_e (mmol/g) was the adsorption capacity and C_0 (mM) and C_e (mM) were, respectively, the initial and equilibrium metal concentrations. V (L) was the solution volume and m (g) was the weight of adsorbent. The Langmuir model considered several assumptions like the adsorption was localized, all the active sites on the surface had similar energies, there was no interaction between adsorbed molecules and the limiting reaction step was the surface as in heterogeneity of the adsorption sites [31].

2.4. Catalyst preparation and reaction

Fe-MCM-41 samples were subjected to copper adsorption using Cu^{+2} concentration of 59.6 ppm, pH 5.5 and temperature 323 K since we found that highest percentage of adsorption takes place under these conditions. We found that Fe-MCM-41(90) showed highest amount of copper loading (Table 6). The oxidation of adamantane with hydrogen peroxide was carried out in a glass batch reactor fitted with a condenser. A known amount of substrate (0.34 g of adamantane, 2.5 mmol), H_2O_2 (0.85 ml, 5.0 mmol), catalyst (Fe-MCM-41(90)–Cu(59.6), 25 mg) and acetonitrile (40 g) were taken in a two-necked round-bottomed flask immersed in an oil bath and fitted with a water condenser. The reactions were conducted at 333 K for 3 h. The identities of the oxidation products were confirmed by GC analysis (Simadzu 17A) with a FID detector using capillary column (ZB5).

2.5. Physico-chemical characterization

The BET surface area, average pore diameter and pore volume of the prepared Fe-MCM-41 samples and Cu(II) adsorbed Fe-MCM-41 samples were determined by multipoint N_2 adsorption–desorption method at liquid N_2 temperature (77 K) by an ASAP 2020 (Micromeritics). Hitachi S3400N recorded the SEM. A JASCO FT-IR-5300 spectrophotometer recorded FT-IR spectra for samples in KBr matrix in the range of 4000–400 cm^{-1}. The diffused reflectance UV–vis spectra were recorded in VARIAN CARY 100 spectrophotometer.

Table 1
Structural parameters of spherical Fe-MCM-41(xx).

Samples with (Si/Fe) ratio	Fe content in the sample (mmol/g)	Surface area (m^2/g)	Pore diameter (nm)	Color of sample
MCM-41	0	1025	2.7	White
Fe-MCM-41(20)	0.48	647	2.2	Beige
Fe-MCM-41(50)	0.36	725	2.2	Beige
Fe-MCM-41(70)	0.18	742	2.3	Beige
Fe-MCM-41(90)	0.101	780	2.4	Beige

3. Results and discussion

3.1. Spherical Fe-MCM-41

As displayed in Table 1, the decrease in pore diameter from 24 Å for Fe-MCM-41(90) to 22 Å for Fe-MCM-41(20) may be attributed to greater tension experienced by the sample with higher Si/Fe atom ratios. Introducing iron into the silicate structure results in the generation of tension of various degrees. This is due to the different bond lengths and angles between Si–O–Si and Si–O–Fe and similarly the difference between the ionic radii of Si^{4+} and Fe^{3+}. The closer the ionic radii lesser is the tension. It is reported that with increase in loading of iron, the silica framework experiences greater tension and increase in wall thickness which leads to disorderness of the structure [32]. The synthesis and characterization of Cu, Co and Fe incorporated spherical MCM-41 and the acidic character has been reported [14]. Surface area increased from 647 to 780 m^2/g with increase in Si/Fe. The color of as-made Fe-MCM-41(xx) samples was beige with fine texture.

The UV–vis diffuse reflectance spectra of Fe-MCM-41(xx) exhibited a strong absorption band in the wavelength range of 220–260 nm (Fig. 1), which is assigned to tetra-coordinated Fe^{3+} species (219 and 255 nm). These samples also demonstrated weaker absorption bands above 400 nm, which was attributed to hexa-coordinated Fe^{3+}. No significant difference was found in the UV–vis DRS by changing the weight percentage of iron, indicating that Fe was successfully incorporated into the silica network. The FT-IR spectra of Fe-MCM-41(50) exhibits a broad band in the hydroxyl region between 3700 and 3000 cm^{-1} with a max. at 3432 cm^{-1} (Fig. 2a). This band can be assigned to adsorbed water molecules. Various C–H stretching vibrations appeared at 2840 and 2925 cm^{-1} due to the presence of organic surfactant molecules.

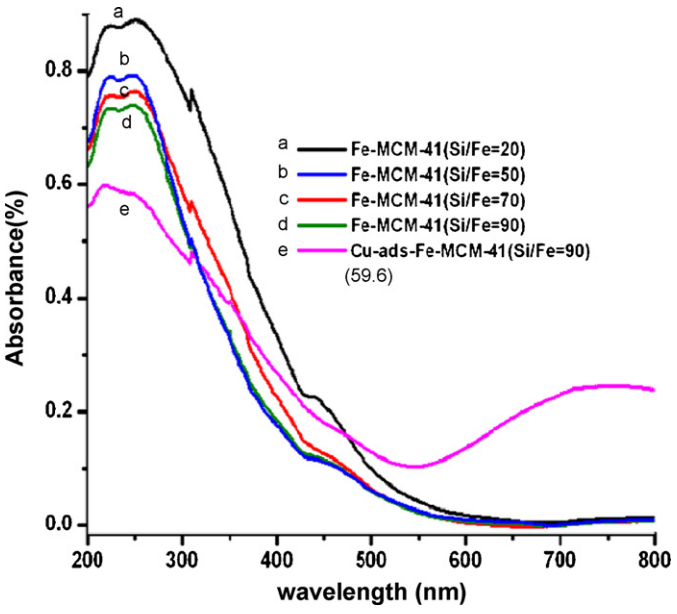

Fig. 1. UV–vis DRS spectra of Fe-MCM-41(xx) samples with various Si/Fe ratios and Cu-adsorbed Fe-MCM-41 (Si/Fe = 90).

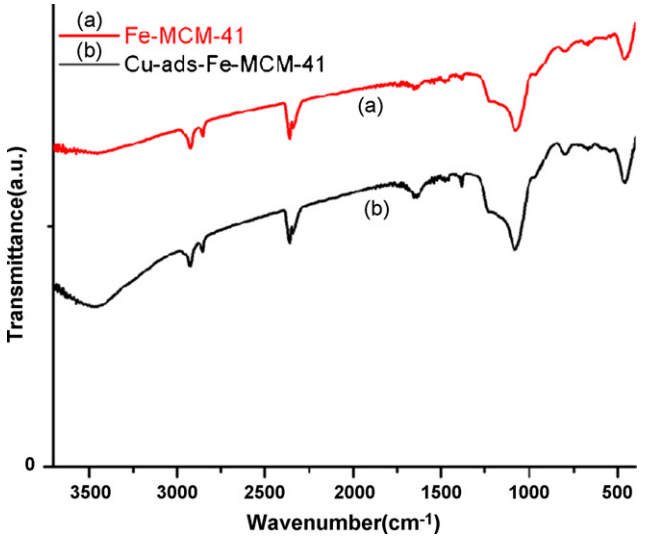

Fig. 2. FT-IR spectra of Fe-MCM-41(90) (a) and Fe-MCM-41(90)–Cu(59.6) (b).

3.2. Cu^{2+} adsorption and iron loading

The Cu^{2+} adsorption was investigated by taking Fe-MCM-41(xx) samples. Increasing Si/Fe atom ratios led to increase in Cu^{2+} adsorption (Fig. 3). Results obtained by AAS reported higher percentage of adsorption of Cu^{2+} ions by Fe-MCM-41(90) (81%) with Cu (59.6 ppm). The change in parameters like concentration, temperature and pH of copper solution controls to the extent of adsorption. The copper adsorbed Fe-MCM-41(90), having lower iron content

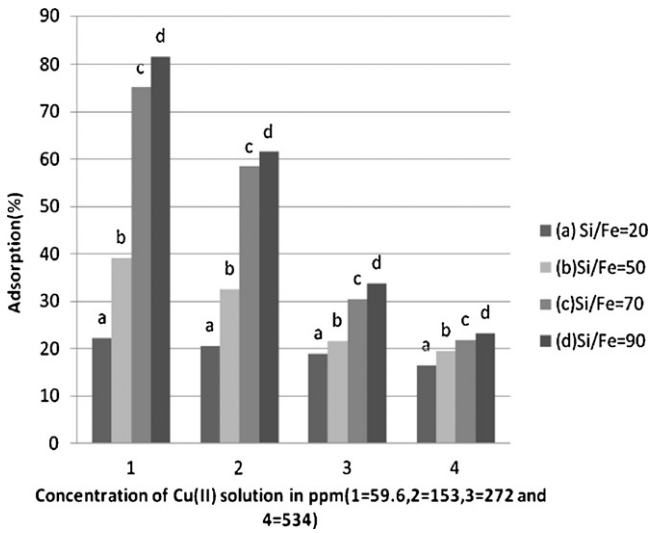

Fig. 3. Adsorption of Cu^{2+}(yy) on Fe-MCM-41(xx).

Table 2
Structural parameters of copper loaded Fe-MCM-41(xx) with varying copper concentrations.

Fe-MCM-41(xx)–Cu(59.6) Si/Fe atom ratio(xx)	Fe-content (mmol/g)	Surface area (m^2/g)	Pore diameter (nm)	Cu content (mmol/g)	Sample color
20	0.46	482	2.1	0.80	Bluish white
50	0.18	548	2.2	1.36	Bluish white
70	0.13	595	2.4	2.43	Light blue
90	0.101	652	2.6	2.72	Light blue

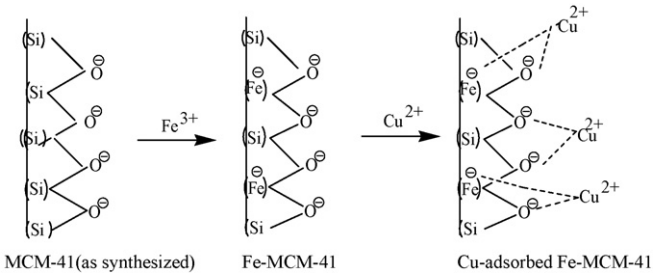

Scheme 1. Possible mechanism for the adsorption of Cu^{2+} on Fe-MCM-41.

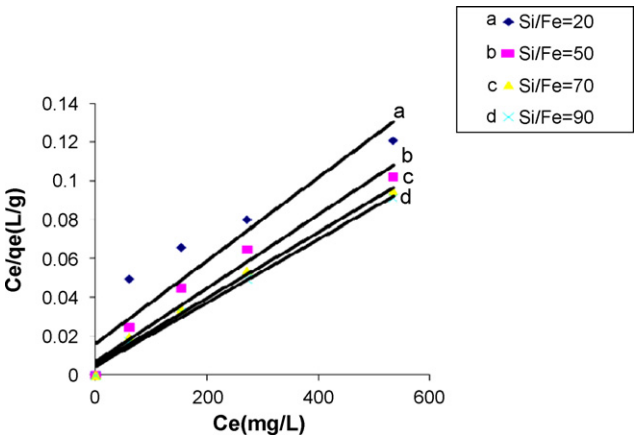

Fig. 4. Langmuir adsorption data for copper adsorption onto Fe-MCM-41(xx).

displayed larger surface area (652 m^2/g) and pore diameter (25 Å) compared to higher iron loading (Table 2). The pore diameter of the Fe-MCM-41(90) was found to be 24 Å resembling a microporous material but after copper adsorption the pore diameter of the Fe-MCM-41(90)–Cu(59.6) increased to 26 Å which may be attributed to Cu–O–Fe and Cu–O–Si bonding as given in Scheme 1 [8].

The analysis of the isotherm data was important to develop an equation to which accurately represented the result and which could be used for design purposes. In order to investigate the sorption isotherm, two equilibrium models were analyzed, the Langmuir and the Freundlich adsorption isotherms. The Langmuir model (Fig. 4) is often used to describe sorption of a solute from a liquid solution as Eq. (2):

$$\frac{C_e}{q_e} = \frac{1}{Q_0 b} + \frac{C_e}{Q_0} \quad (2)$$

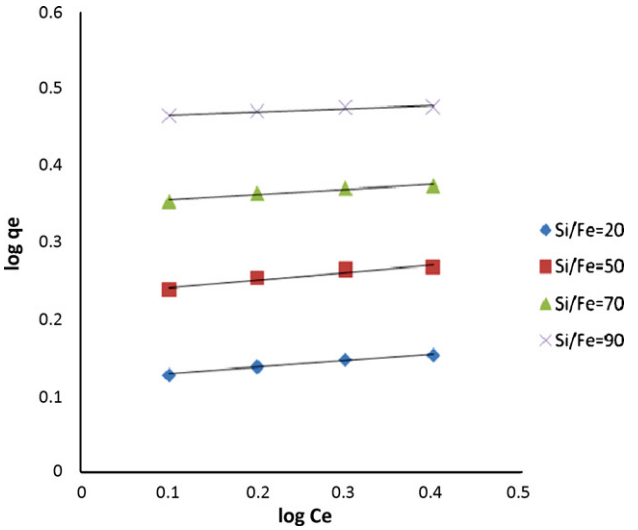

Fig. 5. Freundlich adsorption data for Cu^{2+} adsorption on Fe-MCM-41 samples.

where C_e is the concentration of Cu^{2+} in the solution at equilibrium (mg/L), q_e is the amount of Cu^{2+} adsorbed per unit mass of Fe-MCM-41 (mg/g), Q_0 is the max. uptake of Cu^{2+}/unit mass of Fe-MCM-41 and b is the Langmuir constant.

The efficiency of the adsorption has been predicted by the dimensionless equilibrium parameter R_L, which was defined by Eq. (3):

$$R_L = \frac{1}{1 + bC_0}, \quad (3)$$

where C_0 was the initial concentration of copper in the solution (mg/L). The adsorption was considered to be irreversible when $R_L = 0$, favorable when R_L was between 0 (Henry's law) and 1 (Langmuir form), linear when $R_L = 1$, and unfavorable when $R_L > 1$ (Table 2).

The Freundlich isotherm was mostly used to describe the adsorption of inorganic and organic components in solution (Fig. 5). This fairly satisfactory empirical could be used for nonideal sorption that involves heterogeneous sorption and was expressed as Eq. (5):

$$Q_e = K_F (C_e)^{1/n} \quad (4)$$

the logarithmic form is

$$\log q_e = \log K_F + n \log C_e \quad (5)$$

Table 3
Constants of Eqs. (2)–(4) derived from the list of corresponding models to expt. data.

Fe-MCM-41(xx)–Cu(59.6) Si/Fe ratio(xx)	Langmuir constants		Freundlich constants	
	b (L/mg)	R_L	K_F (mg/g) (mg/L)^n	n
20	0.0089	0.24	2.21	1.54
50	0.0063	0.39	1.01	1.90
70	0.0060	0.53	0.99	1.96
90	0.0057	0.74	1.01	1.99

where C_e and q_e have the same meaning as in Langmuir isotherm and K_F is the Freundlich constant related to the adsorption capacity having dimension (mg/g) $(mg/L)^n$. Adsorption is considered to be satisfactory when the value of Freundlich constant n is between 1 and 10. The constant n is dimensionless and represents energetic heterogeneity of the adsorption sites. The values of Langmuir constants Q_0 and b and Freundlich constants n and K_F are listed in Table 3.

As indicated by the UV–vis DRS spectra (Fig. 1) the copper adsorbed Fe-MCM-41 showed a broad band between 500 and 900 nm, centered at about 775 nm or 12900 cm^{-1}. According to Lever [33], the adsorption band arising from the d–d transition in Cu^{2+} ions in an octahedral coordination sphere with elongated axial Cu–O distances appear at 12200 cm^{-1}. Thus, the peak at 12900 cm^{-1} in this case may be assigned to the same transition. The FT-IR spectra as shown in Fig. 2b displayed almost same spectra for Fe-MCM-41(20, 50,70 and 90) to copper adsorbed Fe-MCM-41(50) excepting a slight shift of some bands. The bands at 3432 and 2923 cm^{-1} shift to 3468 and 2925 cm^{-1}, respectively, due to template-to-template interaction with Cu^{2+}. A broad band at 1653 cm^{-1} assigned to Si–OH and Fe–OH vibrations was shifted to 1638 cm^{-1} with more broadening and higher intensity depicting effective adsorption at surface. A band at 1077 cm^{-1} in adsorbent Fe-MCM-41 shifted to 1080 and 800 cm^{-1} shifted to 799 cm^{-1}, corresponded to asymmetric and symmetric Si–O stretching vibrations, respectively.

We can conclude here that spherical Fe-MCM-41(90) exhibited highest surface area and pore diameter among all the iron modified MCM-41 samples. This sample also showed highest copper adsorption capacity under all the concentration of copper, at pH 5.5 and temperature 323 K.

3.3. Parameters affecting Cu^{2+} loading onto Fe-MCM-41

The adsorption of Cu^{2+} significantly increased with increased temperature as shown in Fig. 6. The factors responsible for effective adsorption such as uniform activation energy of adsobates on the surface and the intra-particle diffusion were favored by higher temperature [34]. The fact that adsorption increased with increase in temperature, established the chemical bonding nature between Cu^{2+} and Fe-MCM-41. The variation of pH greatly influenced the amount of Cu^{2+} loading and was highest at pH 5.5 (Fig. 7). As the higher pH limit for stability of mesoporous MCM-41(8–10), all the experiments were carried out below the range [17,30]. In lower pH ranges, the loading was restricted due to interference of H^+ ions liberated from acid. The optimum adsorption takes place in the pH range of 5–6. Above this pH, the adsorption of Cu^{2+} decreased, which was due to interaction of hydroxyl ions liberated from alkali to that of adsorbed Cu^{2+} ion present on the surface of Fe-MCM-41 [35].

The effect of concentration of Cu^{2+} on adsorption onto Fe-MCM-41 was explained on the basis of Gibbs adsorption isotherm, according to which the extent of adsorption of an electrolyte (Γ_2)

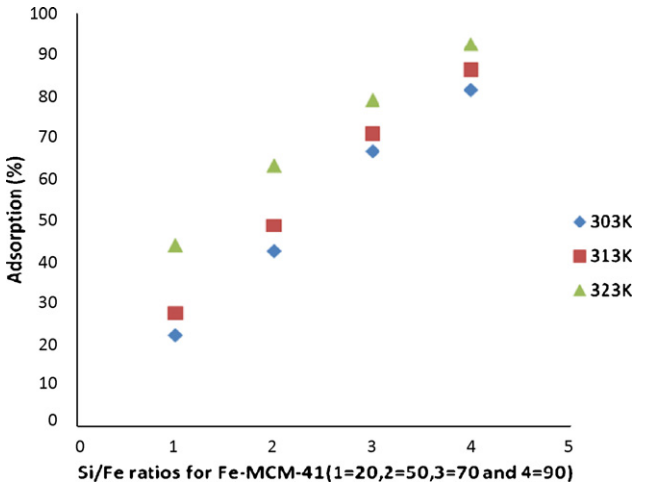

Fig. 6. Adsorption of Cu^{2+} on Fe-MCM-41(xx) at various temperatures.

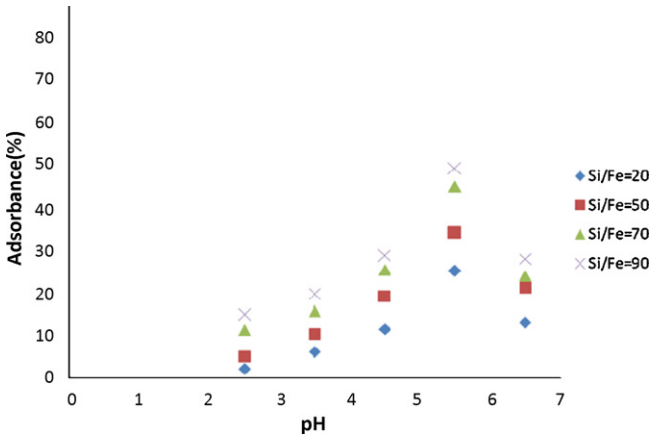

Fig. 7. Adsorption of Cu^{2+} on Fe-MCM-41(xx) at various pH (2.5, 3.5, 4.5, 5.5 and 6.5).

in a solution can be expressed as Eq. (6):

$$\Gamma_2' = \frac{n_2 - (n_1 n_2^0 / n_1^0)}{\sigma} \quad (6)$$

where n_1^0 and n_2^0 were the number of moles of the liquid and the electrolyte, respectively, present in the bulk of solution and n_1 and n_2 were the amount of liquid and electrolyte present at the surface. The surface tension was designated as σ. The adsorption was favorable for a positive value of Γ_2 and unfavorable for a negative values of Γ_2 [36].

At higher concentrations of Cu^{2+} the value of $n_2^0 > n_2$ and n_1^0 was nearly equal to n_1. Hence, Γ_2 attained higher negative value which reduced the extent of adsorption. The SEM analysis of Fe-

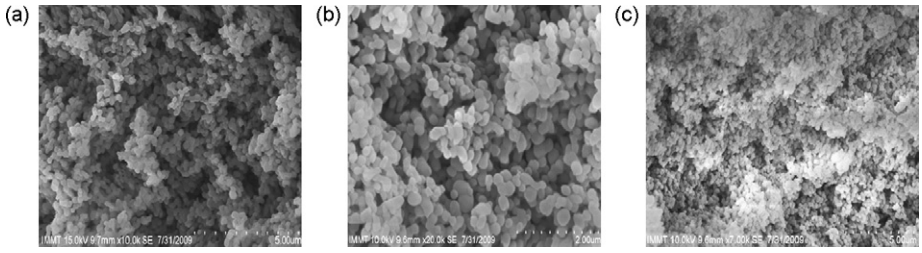

Fig. 8. SEM of (a) Fe-MCM-41(90), (b) Fe-MCM-41(90)–Cu(272) and (c) Fe-MCM-41(90)–Cu(59.6).

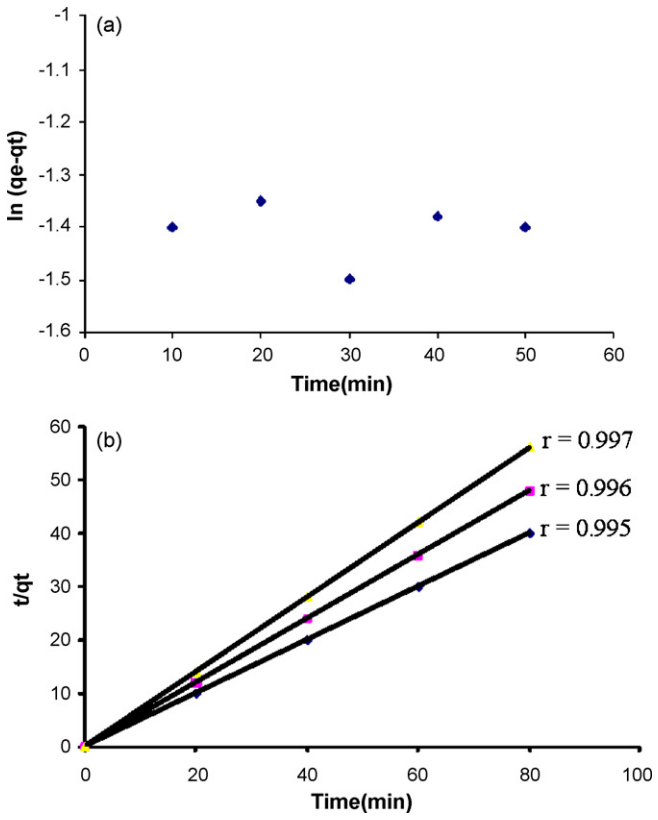

Fig. 9. Kinetic study of Cu(59.6) adsorption on Fe-MCM-41(90): (a) pseudo-first-order model and (b) pseudo-second-order model (C_0 values for lines, 1 = 59.6 ppm, 2 = 153 ppm and 3 = 272 ppm).

MCM-41 with Si/Fe = 90 (Fig. 8a) and samples treated with varying Cu(II) concentrations, i.e., 272 ppm (Fig. 8b) and 59.6 ppm (Fig. 8c) supported the reports of AAS investigations.

3.4. Copper adsorption kinetics

The adsorption rate has been analyzed by taking the pseudo-first-order and pseudo-second-order equations [37,38], respectively.

The pseudo-first-order rate expression can be expressed as:

$$\ln(q_e - q_t) = \ln q_e - k_1 t \quad (7)$$

where q_e is the sorption capacity at equilibrium (mg/g); q_t is the sorption capacity at time t (mg/g) and K_1 is the pseudo-first-order kinetic constant (min^{-1}).

Pseudo-second-order rate equation may be expressed as:

$$\frac{dq_t}{dt} = k_2(q_e - q_t)^2 \quad (8)$$

where K_2 is the pseudo-second-order kinetic constant, expressed in g $mmol^{-1}$ min^{-1}. The linearised form of the above equation yielded:

$$\frac{t}{q_t} = \frac{1}{k_2 q_e^2} + \frac{t}{q_e} \quad (9)$$

linear parameters of Eqs. (7) and (9) are commonly used to check the validity of these models. The apparent lack of linear behaviour describe the kinetic profile not suitable for pseudo-first-order model Fig. 9(a). Rather, rates of Cu(II) adsorption on Fe-MCM-41 are more accurately described by the pseudo-second-order equation as shown in Fig. 9(b). Table 4 summarises the calculated parameters q_e and K_2 for each initial copper concentrations C_0; regression coefficients r obtained from linear fits indicate a good correlation.

Table 4
The pseudo-second-order rate constant values at different initial concentrations of copper removal by Fe-MCM-41(90).

C_0 (mg/L)	q_e (mg/g)	K_2 (g mol^{-1} min^{-1})	r
59.9	0.84	0.23	0.997
153	0.68	0.62	0.996
272	0.33	1.31	0.995

Table 5
Thermodynamic parameters for Cu(II) adsorption on Fe-MCM-41(90) at pH 5.5.

Temperature (K)	ΔG^0 (kJ/mole)	ΔS^0 (kJ/mole)	ΔH^0 (kJ/mole)	R^2
303	−8.24	0.1180		
313	−10.2	0.1168	27.54	0.98
323	−11.6	0.1176		

3.5. Changes of thermodynamic parameters with temperature

The spontaneity of adsorption and the solid–solution interface interactions can be explained by thermodynamic parameters (ΔH^0), (ΔS^0) and (ΔG^0). These parameters are calculated using the van't Hoff and Gibb's equations (10) and (11), respectively:

$$\Delta G^0 = -RT \ln K_a \quad (10)$$

$$\Delta S^0 = \frac{\Delta H^0 - \Delta G^0}{T} \quad (11)$$

K_a is the equilibrium constant of adsorption.

The enthalpy change, ΔH^0 is determined from the plot of $\ln K_a$ vs. $1/T$ (as $d \ln K_a/dT = \Delta H^0/RT^2$). The values of ΔS^0 and ΔG^0 are determined from Eqs. (10) and (11). As shown in Table 5, the decreased value of ΔG^0 from −8.24 kJ/mole (303 K) to −11.6 kJ/mole (323 K) indicated increased adsorption with increase in temperature. Fig. 10 also indicates a good relation with the regression coefficient R^2 (0.98) with a linear form.

3.6. Catalytic reaction

It has been reported by Trissa et al. [29] that the optimum conditions for adamantine oxidation are as follows: adamantane to oxidant ratio (mol:mol) (1:2), temperature 333 K and time 3 h. For evaluating the activities of our catalysts and making a comparison between them, we have maintained similar experimental conditions. Among all the catalysts Fe-MCM-41(90)–Cu(59.6) showed highest adamantane conversion and selectivity to the products. The formation of 1-adamantanol and 2-adamantanone were 54% and 48%, respectively, against 25% and 22.8% in case MCM-41 (Table 6).

The mechanism for oxidation of adamantane with H_2O_2 with Cu-adsorbed Fe-MCM-41 is presumed to be of a free radical type.

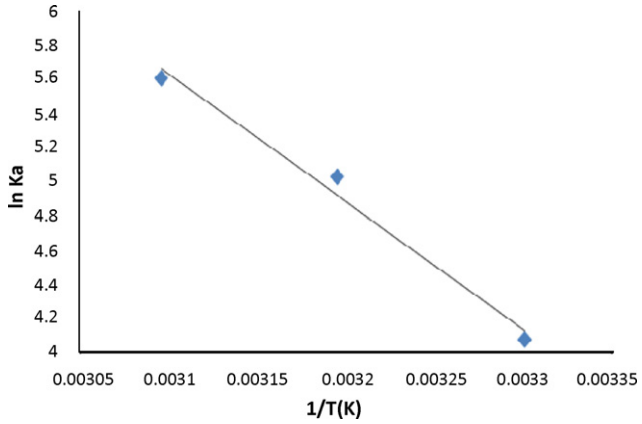

Fig. 10. Van't Hoff plot for Cu(59.6) adsorption on Fe-MCM-41(90).

Table 6
Oxidation of adamantine over various catalysts.

Catalyst used	Cu content (mmol/g)	Conversion (wt.%)	Product selectivity	
			1-adamantanol	2-adamantanone
MCM-41	–	14.1	22. 8	25.0
Fe-MCM-41(90)	–	14.3	28.4	25.5
Fe-MCM-41(50)-Cu(59.6)	1.36	18.6	36.2	34.5
Fe-MCM-41(70)-Cu(59.6)	2.43	28.6	45.4	41.5
Fe-MCM-41(90)-Cu(59.6)	2.72	32.5	54.8	48.6

Reaction conditions: catalyst wt.% = 25 mg, adamantane = 0.34 g (0. 25 mol), H_2O_2 (oxidant) = 0.85 ml (0.25 mol), acetonitrile (solvent) = 40 g (0.5 mol), temperature = 60 °C and reaction time = 3.0 h.

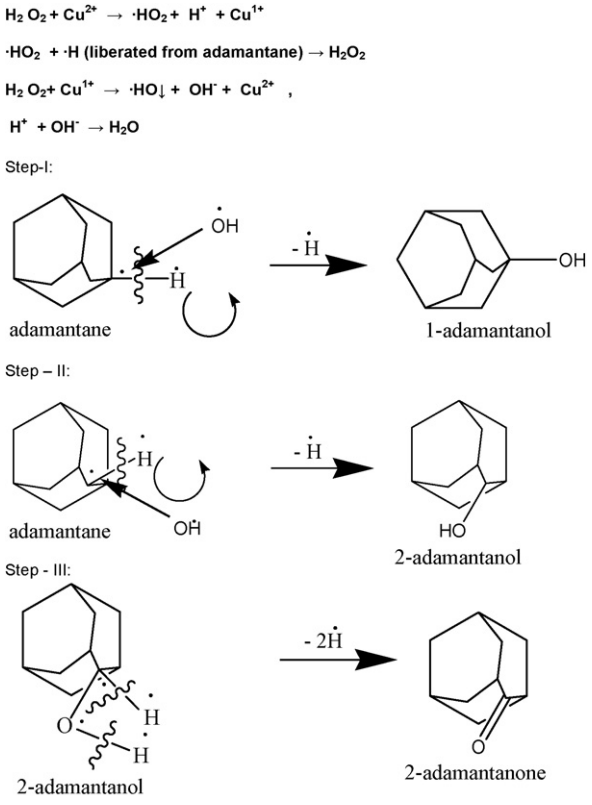

Scheme 2. Possible mechanism for oxidation of adamantane.

The reaction mechanism involving a radical species was proposed from ESR and kinetic data [39]. The catalysts initially abstract the hydrogen of adamantane to form the adamantyl radical. The adamantyl radical formed promotes the successive formation of the key intermediates, such as adamantyl radical and hydroperoxide species. This step is promoted mainly in presence of Cu^{2+} which facilitates the formation of HO_2-free radical by itself getting reduced to Cu^{1+} which reacts with H_2O_2 forming $^{\bullet}OH$ radical. This radical attacks adamantane at 1 and 2 positions simultaneously forming 1-adamantanol and 2-adamantanol. Between the two products, the later is highly energetically unstable and liberates H_2 by taking one hydrogen atom from the same position, thus producing 2-adamantanone. This agrees to the fact that both 1-adamantanol and 2-adamantanone are formed at simultaneously. The proposed mechanism for the oxidation reaction is represented in Scheme 2 [40].

4. Conclusions

Fe-MCM-41(90) was found to be an efficient adsorbent for removal of Cu^{2+} from aqueous solution. The optimum adsorption (81%) occurs at a temperature of 323 K, pH 5.5 and Cu^{2+} concentration 59.6 ppm. The copper enriched sample [Fe-MCM-41(90)–Cu(59.6)] can be efficiently used as a catalyst for the oxidation of adamantane in presence of hydrogen peroxide. The sample exhibits a 32.5% conversion with 54.8% selectivity against only 14% conversion in absence of any catalyst. Our process of oxidation adamantane using copper loaded Fe-MCM-41 is simple, cost effective and eco-friendly.

References

[1] J. Aaseth, T. Norseth, Handbook on the toxicity of Metals, Elsevier, 1986, pp. 233–257.
[2] A. Celeki, M. Yavuzatmaca, H. Bozkurt, An eco-friendly process: predictive modeling of copper adsorption from aqueous solution on *Spirulina platensis*, J. Hazard. Mater. 173 (2010) 123–129.
[3] N.P. Cheremisinoff, Handbook of Water and Wastewater Treatment Technologies, Butterworth and Heinemann, 2002.
[4] C.T. Kresge, M.E. Leonowicz, W.J. Roth, J.C. Vartuli, J.S. Beck, Ordered mesoporous molecular sieves tailored using different synthesis conditions, Nature 359 (1992) 710–713.
[5] S.K. Bhargava, D.B. Akolekar, Adsorption of NO and CO over transition metal incorporated mesoporous catalytic materials, J. Colloid Interf. Sci. 281 (2005) 171–178.
[6] Y.M. Xu, R. Shu Wang, F. Wu, Surface characters and adsorption of Pb(II) onto Ti-MCM-41, J. Colloid Interf. Sci. 209 (1999) 380–385.
[7] A. Benhamou, M. Baudu, Z. Derriche, J.P. Basly, Aqueous heavy metals removal on amine-functionalised Si-MCM-41 and Si-MCM-48, J. Hazard. Mater. 171 (2009) 1001–1008.
[8] K.F. Lam, X. Chen, G. McKay, K.L. Yeung, Anion effect on Cu^{2+} adsorption on NH_2-MCM-41, Ind. Eng. Chem. Res. 47 (2008) 9376–9383.
[9] A.M. Showkat, Y.-P. Zhang, M.S. Kim, A.I. Gopalan, K.R. Reddy, K.-P. Lee, Analysis of heavy metal toxic ions onto amino-functionalized ordered mesoporous silica, Bull. Kor. Chem. Soc. Eng. 28 (2007) 1985–1992.
[10] K. Okumura, K. Nisigaki, M. Niwa, Prominent catalytic activity of Ga-containing MCM-41 in the Friedel–Crafts alkylation, Micropor. Mesopor. Mater. 44–45 (2001) 509–516.
[11] V.R. choudhary, S.K. Jana, N.S. Patil, Acylation of aromatic compounds using moisture insensitive $InCl_3$ impregnated mesoporous Si-MCM-41 catalyst, Tetrahedron Lett. 43 (2002) 1105–1107.
[12] L. Zhang, T. Sun, Y. Ying, Oxidation catalysis over functionalized metalloporphyrins fixated within ultralarge-pore transition metal-doped silicate supports, Chem. Commun. (1999) 1103–1106.
[13] M. Grun, K.K. Unger, A. Matsumoto, K. Tsutsumi, Novel pathways for the preparation of mesoporous MCM-41 materials: control of porosity and morphology, Micropor. Mesopor. Mater. 27 (1998) 207–216.
[14] Y. Wang, Q. Zhang, T. Shishido, K. Takehira, Characterization of iron-containing MCM-41 and its catalytic properties in epoxidation of styrene with hydrogen peroxide, J. Catal. 209 (2009) 186–196.
[15] Y. Wang, Q. Zhang, T. Shishido, K. Takehira, Characterization of iron containing MCM-41 and its catalytic properties in epoxidation of styrene with hydrogen peroxide, J. Catal. 209 (2002) 186–196.
[16] S. Samanta, S. Giri, P.U. Sastry, N.K. Mal, A. Manna, A. Bhaumik, Synthesis and characterization of iron-rich highly ordered mesoporous Fe-MCM-41, Ind. Eng. Chem. Res. 42 (2003) 3012–3018.
[17] A. Szegedi, Z. Konya, D. Mehn, E. Solymar, G. Pal-Borbely, Z. Horvath, L.P. Biro, I. Kiricsi, Spherical mesoporous MCM-41 materials containing transition metals: synthesis and characterisation, Appl. Catal. A: Gen. 272 (2004) 257–266.
[18] K. Watanabe, M. Ogura, Effective factors on solid phase conversion of Fe-containing mesoporous silica into Fe-beta, Micropor. Mesopor. Mater. 114 (2008) 229–237.
[19] W.A. Carvalho, M. Wallau, U. Schuchardt, Iron and copper immobilised on mesoporous MCM-41 molecular sieves as catalysts for the oxidation of cyclohexane, J. Mol. Catal. A 144 (1) (1999) 91–99.
[20] A. Wingen, N. Anastasievi, A. Hollnagel, D. Werner, F. Schuth, Fe-MCM-41 as a catalyst for sulfur dioxide oxidation in highly concentrated gases, J. Catal. 193 (2000) 248–254.

[21] K.F. Lam, X. Chen, C.M. Fong, K.L. Yeung, Selective mesoporous adsorbents for Ag^{+}/Cu^{2+} separation, Chem. Commun. (2008) 2034–2035.
[22] K.F. Lam, K.L. Yeung, G. Mckay, Selective mesoporous adsorbents for $Cr_2O_7^{2-}$ and Cu^{2+} separation, Micropor. Mesopor. Mater. 100 (2007) 191–201.
[23] A. Walcarius, M. Etienne, B. Lebeau, Rate of access to the binding sites in organically modified silicates. 2. Ordered mesoporous silica grafted with amine or thiol groups, Chem. Mater. 15 (2003) 2161–2173.
[24] I. Nowak, B. Kilos, M. Ziolek, A. Lewandowska, Epoxidation of cyclohexene on Nb-containing meso- and macroporous materials, Catal. Today 78 (2003) 487–498.
[25] H. Yoshitake, T. Yokoi, T. Tatsumi, Adsorption behavior of arsenate at transition metal cations captured by amino-functionalized mesoporous silicas, Chem. Mater. 15 (2003) 1713–1721.
[26] S. Rengaraj, Y. Kim, C.K. Joo, J. Yi, Removal of copper from aqueous solution by aminated and protonated mesoporous alumina. Kinetics and equilibrium, J. Colloid Interf. Sci. 273 (2004) 14–21.
[27] A. Kojimo, H. Yamana, K. Okamoto, US Patent AC07C4527FI (2003).
[28] K. Otsuka, JP Patent 6881870 (2005).
[29] J. Trissa, M. Hartmann, S. Ernst, S.B. Halligudi, Oxidation of adamantane by urea hydroperoxide using vanadium complex anchored onto functionalized Si-MCM-41, J. Mol. Catal. A 207 (2004) 131–137.
[30] J.F. Bartoli, K.L. Barch, M. Palacio, P. Battioni, D. Mansuy, Iron polynitroporphyrins bearing up to eight B-nitro groups as interesting new catalysts for H_2O_2 dependent hydrocarbon oxidation: unusual regioselectivity in hydroxylation of alkoxybenzenes, Chem. Commun. (2001) 1718–1719.
[31] I. Langmuir, The adsorption of gases on plain surfaces of glass, platinum and mica, J. Am. Chem. Soc. 40 (1918) 1361–1362.
[32] R.I. Nooney, D. Thirunavukkarasu, Y. Chen, R. Josephs, A.E. Ostafin, Synthesis of nanoscale mesoporous silica spheres with controlled particle size, Chem. Mater. 14 (2002) 4721–4728.
[33] A.B.P. Lever, Inorg. Electronic Spectroscopy, Elsevier, Amsterdam, 1984, pp. 554–560.
[34] S. Rengaraj, C.K. Joo, Y. Kim, J. Yi, Kinetics of removal of chromium from water and electronic process wastewater by ion exchange resins: 1200H, 1500H and IRN97H, J. Hazard. Mater. 102 (2003) 257–264.
[35] K.F. Lam, K.L. Yeung, G. Mckay, A rational approach in the design of selective mesoporous adsorbents, Langmuir 22 (2006) 9632–9641.
[36] R. Rockmann, G. Kalies, Characterization and adsorptive application of ordered mesoporous silica, Appl. Surf. Sci. 253 (2007) 5666–5670.
[37] S. Rengaraj, C.K. Joo, Y. Kim, J. Yi, Kinetics of removal of chromium from water and electronic process wastewater by ion exchange resins: 1200H, 1500H and IRN97H, J. Hazard. Mater. 102 (2003) 257–275.
[38] Y. Kim, C. Kim, I. Choi, S. Rengaraj, J. Yi, Arsenic removal using mesoporous alumina prepared via a templating method, Environ. Sci. Technol. 38 (2004) 924–931.
[39] S. Shinachi, M. Matsushita, K. Yamaguchi, N. Mizuno, Oxidation of adamantane with 1 atm molecular oxygen by vanadium-substituted polyoxometalates, J. Catal. 233 (2005) 81–89.
[40] I.Y. Shchapin, V.V. Vasil'eva, A.I. Nekhaev, E.I. Bagrii, On a possible radical-cation mechanism of the biomimetic oxidationof the saturated hydrocarbon 1,3 dimethyladamantane in a Gif-type system containing a Fe_2 + salt, picolinic acid and pyridine, Kinet. Catal. 47 (2006) 624–637.